Range-Doppler Map Improvement in FMCW Radar for Small Moving Drone Detection Using the Stationary Point Concentration Technique

Junhyeong Park, *Graduate Student Member, IEEE*, Dae-Hwan Jung, Kyung-Bin Bae, and Seong-Ook Park, *Senior Member, IEEE*

***Abstract*— Given the rapidly growing drone market, the development of drone detection radars has become highly important to prevent drones from damaging lives and property. Frequency-modulated continuous-wave (FMCW) radars have been frequently used for drone detection. Among the architectures of FMCW radar, a heterodyne architecture that involves different local oscillators and produces beat signals at the IF stage has often been chosen. The FMCW radar, however, has a chronic problem called leakage. In an earlier study, we proposed the stationary point concentration (SPC) technique to improve the signal-to-noise ratio (SNR) of small drones by reducing the increase in noise floor caused by leakage. We demonstrated that the proposed technique increases the SNR of small hovering drones in the 1-D power spectrum. In this article, we newly analyze the practical problems in the heterodyne FMCW radar system. One is the 2-D noise floor increase in the range-Doppler (r-D) map due to the leakage, and the other is unwanted Doppler shifts. Then, we propose an upgraded theory and realization method of the SPC technique for the detection of the small moving drone by improving the r-D map. We prove that the proposed method not only reduces the 2-D noise floor by mitigating the leakage but also removes the unwanted Doppler shifts by the phase calibration. Consequently, we show that the proposed method increases the SNR of the small moving drone and corrects its velocity information at the same time in the r-D map.**

***Index Terms*— Digital signal processing, frequency-modulated continuous-wave (FMCW) radar, heterodyne architecture, leakage mitigation, noise floor, phase calibration, phase noise, range-Doppler (r-D) map, signal-to-noise ratio (SNR), stationary point concentration (SPC) technique.**

I. Introduction

As DRONE technology and markets have grown, serious incidents have been caused by drones worldwide. In Japan, a man attempted to land a drone with radioactive material on the rooftop of the Japanese prime minister's office [1]. In the USA, a helicopter crashed while trying to avoid a drone [2]. In the U.K., due to sightings of drones at the airport, about 1000 flights were delayed or canceled, and approximately 140 000 passengers were affected [3]. In other words, the threat posed by drones is now a severe problem. In order to prevent incidents by drones, the development of drone detection radar is urgently required.

Frequency-modulated continuous-wave (FMCW) radar is one of the radar types widely used for drone detection [4]–[10]. It has the advantages of low cost, low peak power, and no minimum detectable range compared to pulse radars. There are two typical architectures in the FMCW radar: one is homodyne architecture, and the other is heterodyne architecture. The homodyne FMCW radar has a relatively simple structure. However, it suffers from the problem of dc offset, which saturates the amplifiers and analog-to-digital converter at the baseband and corrupts the baseband signals [11]. In order to prevent the dc offset, the heterodyne architecture has often been employed [10], [12]–[21]. A heterodyne architecture that uses different local oscillators (LOs) and generates the beat signals at the IF stage is one of the most frequently used heterodyne architectures [10], [14]–[21]. This architecture enables us to easily remove not only the dc offset but also unwanted harmonics, intermodulation terms, and spurs in advance at the IF stage. Also, various gain blocks can be simply added. Therefore, this heterodyne architecture reduces the burdens of dealing with the desired beat signals at the baseband.

However, although this heterodyne architecture has many advantages, there is a troublesome inherent problem called leakage in the FMCW radar. In the monostatic configuration, the leakage is caused by insufficient isolation capability of a circulator and antenna mismatch [23]–[25]. In the bistatic configuration, the transmitted signal is directly leaked into the receiver through the transmitter (TX) and receiver (RX) antennas [10], [26]. Also, some objects around the TX and the RX antennas can contribute to the leakage [10], [26], [30], [31]. The leakage power is basically strong, and its relatively poor phase noise raises the noise floor in the power spectrum [10], [23]–[25], [30], [31]. As a consequence, the leakage degrades the detection performance of the FMCW radar.

In a previous work, we proposed the stationary point concentration (SPC) technique to overcome the degradation

Manuscript received July 28, 2019; revised November 24, 2019; accepted December 11, 2019. Date of publication January 13, 2020; date of current version May 5, 2020. This work was supported in part by the Institute for Information and Communications Technology Promotion Grant funded by the Korea Government (MSIT) (Key Technologies Development for Next Generation Satellites) under Grant 2018-0-01658 and in part by KAIST End-Run Program funded by the Korea Government (MSIT) under Grant N11190279. *(Corresponding author: Junhyeong Park.)*

The authors are with the School of Electrical Engineering, Korea Advanced Institute of Science and Technology, Daejeon 34141, South Korea (e-mail: bdsfh0820@kaist.ac.kr; daeman88@kaist.ac.kr; carrierbkb@kaist.ac.kr; soparky@kaist.ac.kr).

Color versions of one or more of the figures in this article are available online at http://ieeexplore.ieee.org.

Digital Object Identifier 10.1109/TMTT.2019.2961911

in detection performance caused by leakage [10]. The SPC technique is a new approach, unlike traditional methods that try to generate the same signal as the leakage and subtract it from the received signal [23]–[25], [27]–[31].

The SPC technique concentrates the phase noise of the leakage on a stationary point of sinusoidal function. By doing this, the magnitude of the phase noise of the leakage is reduced so that the noise floor is decreased. In [10], we positioned small drones in the sky and showed that the SPC technique increases the signal-to-noise ratio (SNR) of the small hovering drones in the power spectrum, the result of just 1-D Fourier transform (FT).

In this article, we focus on practical problems in the heterodyne FMCW radar system and propose the upgraded theory and realization method of the SPC technique for the improvement of the range-Doppler (r-D) map. The r-D map, which is the result of a 2-D FT in the FMCW radar, has been frequently used for moving target detection [4], [32]–[36]. Detecting targets using the r-D map provides information about velocity as well as distance. However, because of the phase noise of the leakage, the 2-D noise floor in the r-D map is also increased, which deteriorates the moving target detection performance. In addition, unwanted Doppler shifts can occur because of imperfections in the radar system. With a poor radar system, the unwanted Doppler shifts can even change from measurement to measurement. These unwanted Doppler shifts distort the velocity information of the moving targets.

Here, we address these practical problems in the heterodyne FMCW radar system. The 2-D noise floor rise in the r-D map by the leakage and the unwanted Doppler shifts caused by system imperfections are analyzed in detail. Then, we theoretically prove that the upgraded SPC technique can resolve the aforementioned problems. The proposed realization method of the upgraded SPC technique for the r-D map improvement is also described. Finally, we demonstrate that the proposed method corrects the unwanted Doppler shifts by calibrating the phase of the beat signals while simultaneously lowering the 2-D noise floor in the r-D map. The experimental results show that the proposed method increases the SNR of small moving drones in the r-D map and provides accurate velocity information at the same time.

For the experiments, a mini-drone, DJI Spark, was used. DJI drones have been widely used as targets and references due to the reliable flight information such as altitude, distance, velocity of the drones, and so on, which are provided by a smart mobile application [5], [9], [10]. All digital signal processes (DSPs) in this article were done with MATLAB.

In Section II, the theory of the common r-D map and the theoretical analyses of the practical problems in the heterodyne FMCW radar are explained. In Section III, the upgraded theory and realization method of the SPC technique for the r-D map improvement are described. The experiments and radar systems used in the experiments are introduced in Section IV. Section V shows all the results and provides the discussions. Then, our conclusion follows in Section VI.

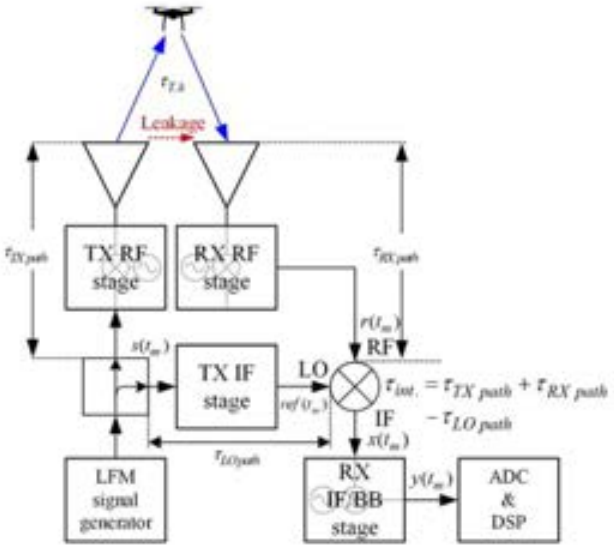

Fig. 1. Block diagram of the heterodyne FMCW radar.

II. Theory of Common r-D Map and Practical Problems in Heterodyne FMCW Radar

A simple block diagram of the heterodyne FMCW radar is shown in Fig. 1. A linear frequency-modulated (LFM) signal, a ramp signal or a chirp signal, which is generated continuously and periodically, is divided into two paths by a splitter. The outputs of the splitter can be defined as follows:

$$s(t_m, m) = A_S \cos(2\pi f_{\mathrm{TX}} t_m + \pi \alpha t_m^2 + \varphi_S(t_m, m)) \quad (1)$$

for $0 < t_m < T$, where $t_m = t - Tm$, and m represents the mth chirp. A_S and f_{TX} are the amplitude and the start frequency of the LFM signal. $\alpha = \mathrm{BW}/T$ is the slope of the chirp. BW and T are the sweep bandwidth and the sweep period. $\varphi_S(t_m, m)$ is the phase noise of the LFM signal. One passes through the TX RF stage that can include cables, LO, mixers, filters, isolators, power amplifiers, and so on. The LO signal in the TX RF stage, $\mathrm{TX\ LO}(t_m, m)$, can be written as follows:

$$\mathrm{TX\ LO}(t_m, m) = A_{\mathrm{TX\,LO}} \cos(2\pi f_{\mathrm{TX\,LO}} t_m + 2\pi f_{\mathrm{TX\,LO}} Tm + \varphi_{\mathrm{TX\,LO}}(t_m, m)) \quad (2)$$

where $A_{\mathrm{TX\,LO}}$, $f_{\mathrm{TX\,LO}}$, and $\varphi_{\mathrm{TX\,LO}}(t_m, m)$ are its amplitude, carrier frequency, and phase noise, respectively. In consideration of $t_m = t - Tm$ and m, the phase term, $2\pi f_{\mathrm{TX\,LO}} Tm$, is introduced. As described in Fig. 2, the phase of the LO signals can be changed along the chirp domain m, whereas the phase of the LFM signal is reset at the end of each chirp. Note that $2\pi f_{\mathrm{TX\,LO}} Tm$ does not exist in the LO expression when considering just t in a general situation. The LFM signal is upconverted and delayed by $\tau_{\mathrm{TX\ path}}$. Then, it is transmitted through the TX antenna in the following form:

$$\begin{aligned}\mathrm{TX\ RF}(t_m, m) &= A_{\mathrm{Transmit}} \cos(2\pi f_{\mathrm{Transmit}}(t_m - \tau_{\mathrm{TX\ path}}) \\ &\quad + \pi\alpha(t_m - \tau_{\mathrm{TX\ path}})^2 \\ &\quad + 2\pi f_{\mathrm{TX\,LO}} Tm + \varphi_S(t_m - \tau_{\mathrm{TX\ path}}, m) \\ &\quad + \varphi_{\mathrm{TX\,LO}}(t_m - \tau_{\mathrm{TX\ path}}, m)) \end{aligned} \quad (3)$$

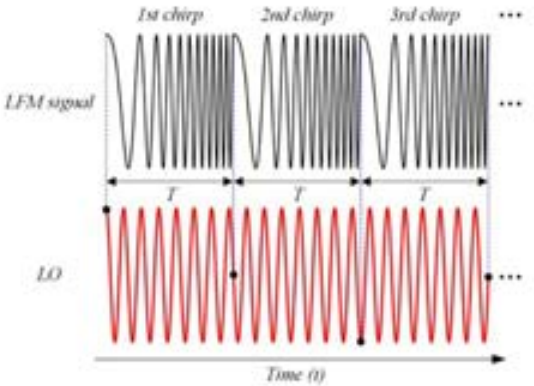

Fig. 2. Phase change of the LO signal along the chirp domain.

where $A_{\text{Transmit}} = A_S A_{\text{TX LO}}/2$, and $f_{\text{Transmit}} = f_{\text{TX}} + f_{\text{TX LO}}$. The transmitted signal is directly leaked into the RX antenna, and the signals reflected by targets are received by the RX antenna. Then, the received signals pass through the RX RF stage that can include low noise amplifiers, isolators, LO, mixers, filters, cables, and so on. The LO signal in the RX RF stage, RX LO(t_m, m), can be written as follows:

$$\text{RX LO}(t_m, m) = A_{\text{RX LO}} \cos(2\pi f_{\text{RX LO}} t_m + 2\pi f_{\text{RX LO}} Tm + \varphi_{\text{RX LO}}(t_m, m)) \quad (4)$$

where $A_{\text{RX LO}}$, $f_{\text{RX LO}}$, and $\varphi_{\text{RX LO}}(t_m, m)$ are the amplitude, the carrier frequency, and its phase noise, respectively. The received signals are then downconverted and delayed by $\tau_{\text{RX path}}$. Therefore, the received signals at the RF port in Fig. 1, $r(t_m, m)$, can be expressed as follows:

$$\begin{aligned} r(t_m, m) &= r_{\text{received leakage}}(t_m, m) + r_{\text{received targets}}(t_m, m) \\ &= A_L \cos(2\pi f_{\text{RX}}(t_m - \tau_{\text{RX path}}) \\ &\quad + \pi a (t_m - \tau_{\text{TX path}} - \tau_{\text{RX path}})^2 \\ &\quad - 2\pi (f_{\text{RX LO}} - f_{\text{TX LO}}) Tm + \theta_L + \varphi_L(t_m, m)) \\ &\quad + \sum_{k=1}^{K} A_{T,k} \cos(2\pi f_{\text{RX}}(t_m - \tau_{\text{RX path}}) \\ &\qquad + \pi a \left(t_m - \tau_{\text{TX path}} - \tau_{\text{RX path}} - \tau_{T,k}\right)^2 \\ &\qquad - 2\pi (f_{\text{RX LO}} - f_{\text{TX LO}}) Tm \\ &\qquad + \theta_{T,k} + \varphi_{T,k}(t_m, m)) \end{aligned} \quad (5)$$

where A_L and $A_{T,k}$, θ_L and $\theta_{T,k}$, and $\varphi_L(t_m, m)$ and $\varphi_{T,k}(t_m, m)$ are the amplitudes, the constant phases, and the phase noises of the leakage and the target LFM signals in $r(t_m, m)$. $f_{\text{RX}} = f_{\text{TX}} + f_{\text{TX LO}} - f_{\text{RX LO}}$, $\theta_{T,k} = -2\pi f_{\text{Transmit}}(\tau_{\text{TX path}} + \tau_{T,k})$, $\theta_L = -2\pi f_{\text{Transmit}} \tau_{\text{TX path}}$, and $\tau_{T,k}$ is the round-trip delay to the kth target. $\varphi_L(t_m, m)$ and $\varphi_{T,k}(t_m, m)$ can be written as follows:

$$\begin{aligned} \varphi_L(t_m, m) &= \varphi_S(t_m - \tau_{\text{TX path}} - \tau_{\text{RX path}}, m) \\ &\quad - \varphi_{\text{RX LO}}(t_m - \tau_{\text{RX path}}, m) \\ &\quad + \varphi_{\text{TX LO}}(t_m - \tau_{\text{TX path}} - \tau_{\text{RX path}}, m) \end{aligned} \quad (6)$$

$$\begin{aligned} \varphi_{T,k}(t_m, m) &= \varphi_S(t_m - \tau_{\text{TX path}} - \tau_{\text{RX path}} - \tau_{T,k}, m) \\ &\quad + \varphi_{\text{TX LO}}(t_m - \tau_{\text{TX path}} - \tau_{\text{RX path}} - \tau_{T,k}, m) \\ &\quad - \varphi_{\text{RX LO}}(t_m - \tau_{\text{RX path}}, m). \end{aligned} \quad (7)$$

The other output of the splitter passes through the TX IF stage that can include cables, amplifiers, filters, isolators, and so on. Then, this signal, ref(t_m, m), can be represented as follows:

$$\begin{aligned} \text{ref}(t_m, m) = A_{\text{ref}} \cos(2\pi f_{\text{TX}}(t_m - \tau_{\text{LO path}}) + \pi a (t_m - \tau_{\text{LO path}})^2 \\ + \varphi_S(t_m - \tau_{\text{LO path}}), m). \end{aligned} \quad (8)$$

Finally, we can extract the IF beat signals, $x(t_m, m)$, by mixing (8) with (5). Note that every mixing process in this article is assumed to be an ideal multiplication. In consideration of moving targets, we put $\tau_{T,k} = 2(R_{o,k} \pm v_k(t_m + Tm))/c$. $R_{o,k}$ and v_k are the initial distance and the radial velocity of the kth target, respectively. All negligible terms are removed in $x(t_m, m)$. The resulting $x(t_m, m)$ is as follows:

$$\begin{aligned} &x(t_m, m) \\ &= x_{\text{IF beat leakage}}(t_m, m) + x_{\text{IF beat targets}}(t_m, m) \\ &= \frac{A_{\text{ref}} A_L}{2} \\ &\quad \times \cos\Bigg(2\pi \Bigg(\overbrace{\underbrace{f_{\text{TX}} - f_{\text{RX}}}_{f_{\text{IF carrier}}} + f_{\text{offset}} + f_{\text{random},t} + \underbrace{\alpha \tau_{\text{int.}}}_{f_{\text{beat leakage}}}}^{f_{\text{IF beat leakage}}(m)}\Bigg) t_m \\ &\quad + \underbrace{2\pi (f_{\text{RX LO}} - f_{\text{TX LO}} + f_{\text{offset}} + f_{\text{random},c}) Tm - \underbrace{\theta_L + \theta_{\text{etc. leak}}}_{\theta_{\text{leakage}}}}_{\theta_{\text{IF leakage}}(m)} \\ &\quad + \varphi_{\text{IF leakage}}(t_m, m)\Bigg) \\ &\quad + \sum_{k=1}^{K} \frac{A_{\text{ref}} A_{T,k}}{2} \\ &\quad \times \cos\Bigg(2\pi \Bigg(\overbrace{\underbrace{f_{\text{TX}} - f_{\text{RX}}}_{f_{\text{IF carrier}}} + f_{\text{offset}} + f_{\text{random},t} + \underbrace{\alpha \tau_{\text{int.}}}_{f_{\text{beat leakage}}} + \underbrace{\alpha \tau_{o,k}}_{f_{\text{beat target},k}}}^{f_{\text{IF beat leakage}}(m)}\Bigg) \\ &\quad \times t_m + 2\pi \Bigg(f_{\text{RX LO}} - f_{\text{TX LO}} + f_{\text{offset}} \\ &\quad + f_{\text{random},c} \pm \underbrace{2 f_{\text{Transmit}} v_k / c}_{f_{d,k}}\Bigg) Tm \\ &\quad \underbrace{-\theta_{T,k} + \theta_{\text{etc. target},k}}_{\theta_{\text{target},k}} + \varphi_{\text{IF target},k}(t_m, m)\Bigg) \end{aligned} \quad (9)$$

where c is the speed of light, $\tau_{o,k} = 2R_{o,k}/c$ is the initial round-trip delay to the kth target, $f_{d,k}$ is the Doppler frequency due to the movement of the targets, and $\tau_{\text{int.}} = \tau_{\text{TX path}} + \tau_{\text{RX path}} - \tau_{\text{LO path}}$ is the total internal delay. $\varphi_{\text{IF leakage}}(t_m, m) = \varphi_S(t_m - \tau_{\text{LO path}}, m) - \varphi_L(t_m, m)$ and $\varphi_{\text{IF target},k}(t_m, m) = \varphi_S(t_m - \tau_{\text{LO path}}, m) - \varphi_{T,k}(t_m, m)$. Also, $\theta_{\text{etc. leak}}$ and $\theta_{\text{etc. target},k}$ are the rest of the constant phases in $x_{\text{IF beat leakage}}(t_m, m)$ and $x_{\text{IF beat targets}}(t_m, m)$, respectively. The practical problems in the heterodyne FMCW radar are

reflected in (9). One is the frequency offset f_{offset}, and the others are the randomly changing frequencies, $f_{\text{random},t}$ and $f_{\text{random},c}$, in the time domain t_m and the chirp domain m, respectively.

Even though the LO based on the phase-locked loop (PLL) is locked, the resulting output carrier frequency has a small frequency offset error. For instance, an LO designed for 10 GHz produces 9.99999 GHz in reality. All LOs in the radar system have this practical issue [37]–[40]. Thus, in practice, it is difficult to completely eliminate the carrier frequency when the downconversions are performed. Through all the upconversions and downconversions in the radar system, the final offset frequency value, which is the result of summation and subtraction of all the offset frequency values, can be close to zero or far away from zero. Even though this frequency offset value can be small in the range domain, it is a relatively large value in the Doppler domain so that it can produce a significant Doppler shift.

In addition, the phase in the beat signals can be changed since all the RF parts can have phase instability. The phase instability is caused by various factors, including temperature and humidity [41], [42]. An unlocked frequency or phase in the PLL can also cause instability. Unwanted phase change frequently occurs in a poor radar system. If the phase is gradually changed with a random slope in a relatively fast time, it can generate a randomly changing frequency $f_{\text{random},t}$ in the time domain.

Likewise, if the phase is gradually changed with a random slope in a relatively slow time, it can generate a randomly changing frequency $f_{\text{random},c}$ in the chirp domain. $f_{\text{random},c}$ is small enough when compared with the other frequency components in the time domain. It may slightly change $f_{\text{IF beat leakage}}(m)$ or the beat frequency of the final beat signal at each mth chirp. However, $f_{\text{random},c}$ can have an impact that cannot be ignored. As a result, the measured velocity information of the targets can change every time the measurement is made.

The IF beat signals are finally downconverted in the RX IF/BB stage. In a common heterodyne FMCW radar, only the IF carrier frequency $f_{\text{IF carrier}}$, which has no information, is removed with the flowing last LO

$$\begin{aligned}\text{LO}_{\text{common}}(t_m, m) = A_{\text{LO}} \cos(&2\pi f_{\text{IF carrier}} t_m + 2\pi f_{\text{IF carrier}} Tm \\ &+ \varphi_{\text{LO}}(t_m, m)) \quad (10)\end{aligned}$$

where A_{LO} and $\varphi_{\text{LO}}(t_m, m)$ are the amplitude and the phase noise of the last LO, respectively. Note that, of course, another frequency offset and another randomly changing frequency may occur in this process. The final signal, $y(t_m, m)$, can be written as follows:

$$\begin{aligned}&y(t_m, m) \\ &= y_{\text{leakage}}(t_m, m) + y_{\text{targets}}(t_m, m) \\ &= A_{\text{leakage}} \cos(2\pi (f_{\text{offset}} + f_{\text{random},t} + f_{\text{beat leakage}}) t_m \\ &\qquad + 2\pi (f_{\text{offset}} + f_{\text{random},c}) Tm + \theta_{\text{leakage}} \\ &\qquad + \varphi_{\text{leakage}}(t_m, m)) \\ &\quad + \sum_{k=1}^{K} A_{\text{target},k} \cos(2\pi (f_{\text{offset}} + f_{\text{random},t} \\ &\qquad + f_{\text{beat leakage}} + f_{\text{beat target},k}) t_m \\ &\qquad + 2\pi (f_{\text{offset}} + f_{\text{random},c} \pm f_{d,k}) Tm \\ &\qquad + \theta_{\text{target},k} + \varphi_{\text{target},k}(t_m, m)) \quad (11)\end{aligned}$$

where $A_{\text{leakage}} = A_{\text{ref}} A_L A_{\text{LO}}/4$ and $A_{\text{target},k} = A_{\text{ref}} A_{T,k} A_{\text{LO}}/4$. $\varphi_{\text{leakage}}(t_m, m) = \varphi_{\text{IF leakage}}(t_m, m) - \varphi_{\text{LO}}(t_m, m)$ and $\varphi_{\text{target},k}(t_m, m) = \varphi_{\text{IF target},k}(t_m, m) - \varphi_{\text{LO}}(t_m, m)$. We can apply the cosine sum identity and the small-angle approximation to (11) [10], [30], [31]. Then, (11) can be rewritten as follows:

$$\begin{aligned}&y(t_m, m) \\ &\approx \underbrace{\begin{aligned}&A_{\text{leakage}} \cos(2\pi (f_{\text{offset}} + f_{\text{random},t} + f_{\text{beat leakage}}) t_m \\ &\qquad + 2\pi (f_{\text{offset}} + f_{\text{random},c}) Tm + \theta_{\text{leakage}}) \\ &\quad - A_{\text{leakage}} \varphi_{\text{leakage}}(t_m, m) \sin(2\pi (f_{\text{offset}} + f_{\text{random},t} \\ &\qquad + f_{\text{beat leakage}}) t_m + 2\pi (f_{\text{offset}} + f_{\text{random},c}) Tm + \theta_{\text{leakage}})\end{aligned}}_{\text{Major cause of the 2 D noise floor rise}} \\ &\quad + \sum_{k=1}^{K} [A_{\text{target},k} \cos(2\pi (f_{\text{offset}} + f_{\text{random},t} + f_{\text{beat leakage}} \\ &\qquad + f_{\text{beat target},k}) t_m \\ &\qquad + 2\pi (f_{\text{offset}} + f_{\text{random},c} \pm f_{d,k}) Tm \\ &\qquad + \theta_{\text{target},k}) \\ &\qquad - A_{\text{target},k} \varphi_{\text{target},k}(t_m, m) \\ &\qquad \times \sin(2\pi (f_{\text{offset}} + f_{\text{random},t} + f_{\text{beat leakage}} \\ &\qquad + f_{\text{beat target, k}}) t_m \\ &\qquad + 2\pi (f_{\text{offset}} + f_{\text{random},c} \pm f_{d,k}) Tm + \theta_{\text{target},k})]. \quad (12)\end{aligned}$$

In order to extract the r-D map, the 2-D FT is applied in (12). Usually, the FT is first applied to the time domain t_m, then FT is applied to the chirp domain m. The resulting 2-D FT includes both the desired terms and the image terms. For convenience in the derivation, we only consider the desired terms. Therefore, the results can be represented as follows:

$$\begin{aligned}&Y(\Omega, \omega) \\ &= Y_{\text{leakage}}(\Omega, \omega) + Y_{\text{targets}}(\Omega, \omega) \\ &\approx A_{\text{leakage}} e^{j\theta_{\text{leakage}}}/2 \\ &\quad \times \{4\pi^2 \delta(\Omega - (\Omega_{\text{offset}} + \Omega_{\text{random},t} + \Omega_{\text{beat leakage}})) \\ &\qquad \times \delta(\omega - (\omega_{\text{offset}} + \omega_{\text{random},c})) \\ &\qquad - e^{-j\pi/2} \Phi_{\text{leakage}}(\Omega - (\Omega_{\text{offset}} + \Omega_{\text{random},t} + \Omega_{\text{beat leakage}}), \\ &\qquad\qquad \omega - (\omega_{\text{offset}} + \omega_{\text{random},c}))\} \\ &\quad + \sum_{k=1}^{K} [A_{\text{target},k} e^{j\theta_{\text{target},k}}/2 \\ &\qquad \times \{4\pi^2 \delta(\Omega - (\Omega_{\text{offset}} + \Omega_{\text{random},t} \\ &\qquad\qquad + \Omega_{\text{beat leakage}} + \Omega_{\text{beat target},k})) \\ &\qquad \times \delta(\omega - (\omega_{\text{offset}} + \omega_{\text{random},c} \pm \omega_{d,k})) \\ &\qquad - e^{-j\pi/2} \Phi_{\text{target},k}(\Omega - (\Omega_{\text{offset}} + \Omega_{\text{random},t} \\ &\qquad\qquad + \Omega_{\text{beat leakage}} + \Omega_{\text{beat target},k}), \\ &\qquad\qquad \omega - (\omega_{\text{offset}} + \omega_{\text{random},c} \pm \omega_{d,k}))\}] \\ &\qquad\qquad (13)\end{aligned}$$

where $\omega_{d,k} = 2\pi f_d T$ and f_d is unambiguous in the range of $-1/2T < f_d < 1/2T$.

In (12), $\varphi_{\text{leakage}}(t_m, m)$, the phase noise of the leakage beat signal, is upconverted to $f_{\text{offset}} + f_{\text{random},t} + f_{\text{beat leakage}}$ in the time domain or to $f_{\text{offset}} + f_{\text{random},c}$ in the chirp domain. Thus, the phase noise manifests itself as a voltage noise or a current noise. In (13), this problematic term is transformed as $-(A_{\text{leakage}} e^{j\theta_{\text{leakage}}} e^{-j\pi/2}/2) \times \Phi_{\text{leakage}}(\Omega - (\Omega_{\text{offset}} + \Omega_{\text{random},t} + \Omega_{\text{beat leakage}}), \omega - (\omega_{\text{offset}} + \omega_{\text{random},c}))$ and becomes the major cause of the 2-D noise floor rise. In addition, the unwanted Doppler shift terms, ω_{offset} and $\omega_{\text{random},c}$, are included in the Doppler domain of the target beat signals. These terms can seriously degrade the accuracy of the measured velocity information of the targets.

III. Proposed Method: Upgraded Theory and Realization Method of SPC Technique for r-D Map Improvement

A. Upgraded Theory of SPC Technique

The upgraded SPC technique for the 2-D scheme is applied after $x(t_m, m)$ is extracted. Unlike the common method, which just uses $f_{\text{IF carrier}}$ for the frequency of the last LO, the upgraded SPC technique for the r-D map uses the exact IF beat frequency of the leakage $f_{\text{IF beat leakage}}(m)$ and the exact IF constant phases of the leakage $\theta_{\text{IF leakage}}(m)$ for the last LO. When we consider multiple chirps for the r-D map, the LO for the upgraded SPC technique can be written as follows:

$$\text{LO}_{\text{SPC}}(t_m, m) = A_{\text{LO}} \cos(2\pi f_{\text{IF beat leakage}}(m) t_m + \theta_{\text{IF leakage}}(m) + \varphi_{\text{LO}}(t_m, m)). \quad (14)$$

If (9) is mixed with (14), then the desired final signal, $z(t_m, m)$, is as follows:

$$\begin{aligned} z(t_m, m) &= z_{\text{leakage}}(t_m, m) + z_{\text{targets}}(t_m, m) \\ &= A_{\text{leakage}} \cos(\varphi_{\text{leakage}}(t_m, m)) \\ &\quad + \sum_{k=1}^{K} A_{\text{target},k} \cos\left(2\pi f_{\text{beat target},k} t_m \pm 2\pi f_{d,k} T m \right. \\ &\quad \left. + \theta'_{\text{target},k} + \varphi_{\text{target},k}(t_m, m)\right) \end{aligned} \quad (15)$$

where $\theta'_{\text{target},k} = \theta_{\text{target},k} - \theta_{\text{leakage}}$. If we apply the cosine sum identity and the small-angle approximation to (15), then $z(t_m, m)$ can be rewritten as follows:

$$\begin{aligned} &z(t_m, m) \\ &\approx A_{\text{leakage}} \\ &\quad + \sum_{k=1}^{K} \left[A_{\text{target},k} \cos\left(2\pi f_{\text{beat target},k} t_m \pm 2\pi f_{d,k} T m + \theta'_{\text{target},k}\right) \right. \\ &\quad - A_{\text{target},k} \varphi_{\text{target},k}(t_m, m) \\ &\quad \left. \times \sin(2\pi f_{\text{beat target},k} t_m \pm 2\pi f_{d,k} T m + \theta'_{\text{target},k}) \right]. \end{aligned} \quad (16)$$

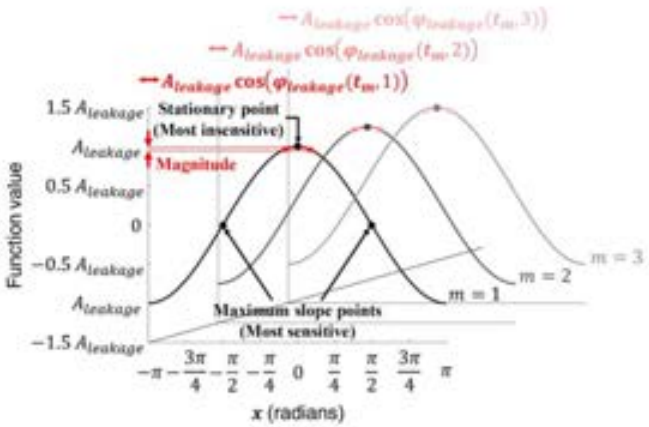

Fig. 3. Phase noise of the leakage concentrated at a stationary point. Multiple chirps are considered.

Finally, applying the 2-D FT to (16) gives

$$\begin{aligned} &Z(\Omega, \omega) \\ &= Z_{\text{leakage}}(\Omega, \omega) + Z_{\text{targets}}(\Omega, \omega) \\ &\approx 4\pi^2 A_{\text{leakage}} \delta(\Omega)\delta(\omega) \\ &\quad + \sum_{k=1}^{K} \left[A_{\text{target},k} e^{j\theta'_{\text{target},k}} / 2 \{ 4\pi^2 \delta(\Omega - \Omega_{\text{beam target},k}) \right. \\ &\qquad \times \delta(\omega \pm \omega_{d,k}) \\ &\qquad \left. - e^{-j\pi/2} \Phi_{\text{target},k}(\Omega - \Omega_{\text{beat target},k}, \omega \pm \omega_{d,k}) \} \right]. \end{aligned} \quad (17)$$

In (15)–(17), there is no longer any major term to cause the 2-D noise floor rise in (12). The leakage is left as just a dc. Even though we do not use the approximation, the only remaining term associated with the phase noise of the leakage is a cosine term in (15). The cosine function envelops the phase noise of the leakage. This situation is described in Fig. 3.

In the common method, since the leakage beat signal $y_{\text{leakage}}(t_m, m)$ has frequencies and phases, the phase noise of the leakage trembles at every point, including the maximum slope points of the cosine function. In contrast, with the proposed method, the frequency and the constant phase of the leakage beat signal are removed for each mth chirp. In other words, the proposed method calibrates the frequency and the constant phase of the leakage beat signal to zero. As a result, the phase noise of the leakage trembles only at the stationary point in each mth chirp. Thus, the magnitude of the phase noise is considerably reduced in both the time domain and the chirp domain, and this leads to a decrease in the 2-D noise floor. In addition, note that because the unwanted phase terms, $2\pi(f_{\text{offset}} + f_{\text{random},c})Tm$, are caused by the radar system, $x_{\text{IF beat targets}}(t_m, m)$ also has these unwanted phase terms as in $x_{\text{IF beat leakage}}(t_m, m)$. The proposed method puts the exact IF constant phases of the leakage, $\theta_{\text{IF leakage}}(m)$, which includes the unwanted phase terms, for the phases of the last LO. Thus, the phase information is correctly calibrated by removing the unwanted phases in every chirp, and this leads to the elimination of the unwanted Doppler shift terms, ω_{offset} and $\omega_{\text{random},c}$ in (17).

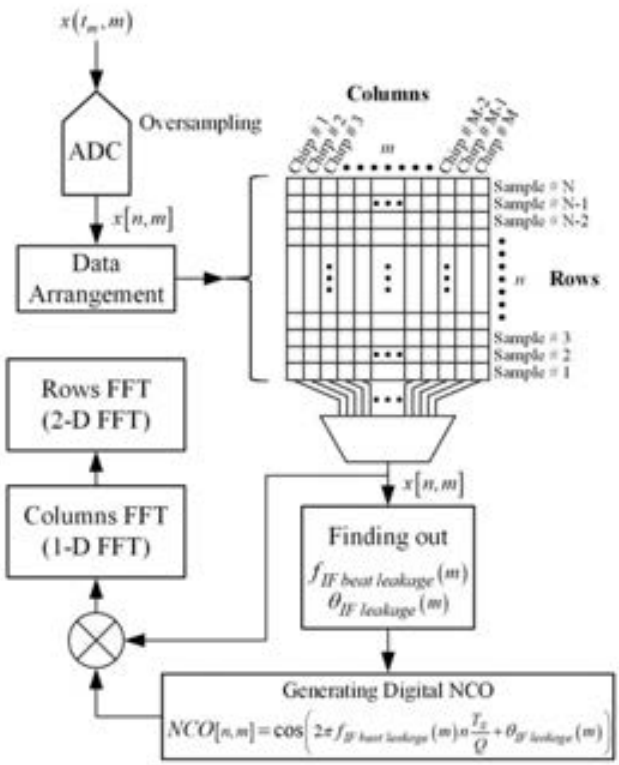

Fig. 4. Block diagram of the proposed method for the extraction of the improved r-D map.

As a consequence, the proposed method improves the r-D map by increasing not only the SNR but also the accuracy of the velocity information of the moving targets at the same time.

Regarding correction capability, although the proposed method that is based on the SPC technique also provides correction in distance information, this feature was verified in our previous work with small static drones [10]. Thus, in this article, we focus on the correction of the velocity information with a small moving drone.

B. Realization Method of Upgraded SPC Technique

The upgraded SPC technique for the r-D map can be realized by strategic frequency planning and DSPs without any additional hardware parts. The proposed realization method of the upgraded SPC technique to produce the improved r-D map is shown in Fig. 4. Under the strategic frequency planning in [10], $f_{\text{IF beat leakage}}(m)$ is placed around a quarter point of the oversampled frequency domain, QF_S. Then, the IF beat signals, $x(t_m, m)$, are oversampled by an analog-to-digital converter (ADC). The oversampled IF beat signals, $x[n, m]$, can be written as follows:

$$\begin{aligned} x[n,m] &= x_{\text{IF beat leakage}}[n,m] + x_{\text{IF beat targets}}[n,m] \\ &= \frac{A_{\text{ref}}A_L}{2}\cos\left(2\pi f_{\text{IF beat leakage}}(m)n\frac{T_S}{Q} + \theta_{\text{IF leakage}}(m) \right. \\ &\quad \left. + \varphi_{\text{IF leakage}}\left(n\frac{T_S}{Q}, m\right)\right) \\ &\quad + \sum_{k=1}^{K}\frac{A_{\text{ref}}A_{T,k}}{2} \\ &\quad \times \cos\left(2\pi\left(f_{\text{IF beat leakage}}(m) + f_{\text{beat target},k}\right)n\frac{T_S}{Q}\right. \\ &\quad + 2\pi\left(f_{\text{RX LO}} - f_{\text{TX LO}} + f_{\text{offset}}\right. \\ &\quad \left. \left. + f_{\text{random},c} \pm f_{d,k}\right)Tm \right. \\ &\quad \left. + \theta_{\text{target},k} + \varphi_{\text{IF target},k}\left(n\frac{T_S}{Q}, m\right)\right) \end{aligned} \tag{18}$$

where $T_S/Q = 1/QF_S$ is the oversampling interval, Q is the oversampling factor, and F_S is the minimum available sampling frequency according to the Nyquist theorem. The oversampled IF beat signals are arranged into a 2-D data matrix. Then, each $x[n, m]$ at the mth chirp passes the following three steps.

First, the fast FT (FFT) is applied with zero padding. We use the following to determine both $f_{\text{IF beat leakage}}(m)$ and $\theta_{\text{IF leakage}}(m)$:

$$\begin{aligned} k_{\text{IF leakage}}(m) &= \underset{\frac{\text{NFFT}}{8} < k < \frac{3\text{NFFT}}{8}}{\arg\max} |X[k,m]|^2 \\ f_{\text{IF beat leakage}}(m) &= \frac{QF_S}{\text{NFFT}}[k_{\text{IF leakage}}(m) - 1] \\ \theta_{\text{IF leakage}}(m) &= \angle X[k_{\text{IF leakage}}] \end{aligned} \tag{19}$$

where $X[k]$ is the result of the NFFT-point FFT of $x[n]$ and NFFT is the total number of real samples and zero pads. $\angle X$ is the phase response of $X[k]$. Note that the peak search range is set to $\text{NFFT}/8 < k < 3\text{NFFT}/8$ by considering the unwanted frequency shift due to f_{offset} and $f_{\text{random},t}$, though we suggested that the peak search range can be $\text{NFFT}/4 < k < \text{NFFT}/2$ in [10].

Second, a digital numerically controlled oscillator (NCO) is generated with the extracted values of $f_{\text{IF beat leakage}}(m)$ and $\theta_{\text{IF leakage}}(m)$. The digital NCO is expressed as follows:

$$\text{NCO}[n,m] = \cos\left(2\pi f_{\text{IF beat leakage}}(m)n\frac{T_S}{Q} + \theta_{\text{IF leakage}}(m)\right). \tag{20}$$

Third, each $x[n, m]$ is multiplied with each digital NCO for mixing. Then, the desired final signal, $\psi[n, m]$, can be represented as follows:

$$\begin{aligned} \psi[n,m] &= \psi_{\text{leakage}}[n,m] + \psi_{\text{targets}}[n,m] \\ &= \frac{A_{\text{ref}}A_L}{4}\cos\left(\varphi_{\text{IF leakage}}\left(n\frac{T_S}{Q}, m\right)\right) \\ &\quad + \sum_{k=1}^{K}\frac{A_{\text{ref}}A_{T,k}}{4} \\ &\quad \times \cos\left(2\pi f_{\text{beat target},k}n\frac{T_S}{Q} \pm 2\pi f_{d,k}Tm \right. \\ &\quad \left. + \theta'_{\text{target},k} + \varphi_{\text{IF target},k}\left(n\frac{T_S}{Q}, m\right)\right). \end{aligned} \tag{21}$$

After all $x[n, m]$ signals at the mth chirp have gone through the above-mentioned processes, we can extract the r-D map by applying the 2-D FFT. If we consider the identity and the

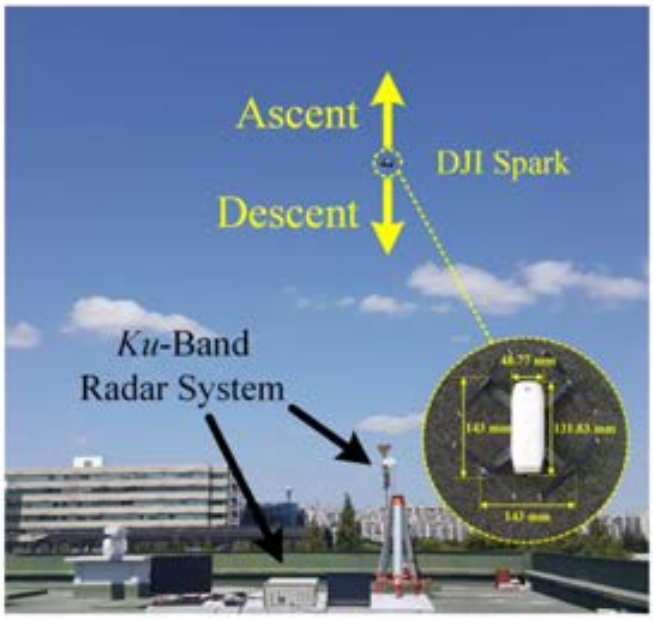

Fig. 5. Scene of Experiment A and the small drone, DJI Spark.

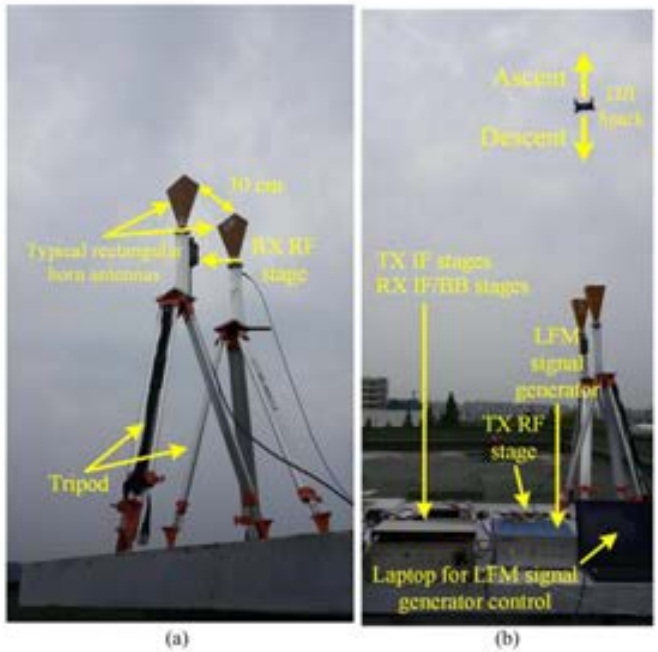

Fig. 6. (a) RF front end of the X-band radar. (b) Scene of Experiment B.

approximation in (16) and (17), (21) can be transformed as follows:

$$\begin{aligned}
&\Psi(\omega_r, \omega_D) \\
&= \Psi_{\text{leakage}}(\omega_r, \omega_D) + \Psi_{\text{targets}}(\omega_r, \omega_D) \\
&\approx A_{\text{ref}} A_L \pi^2 \delta(\omega_r)\delta(\omega_D) \\
&\quad + \sum_{k=1}^{K} \left[\frac{A_{\text{ref}} A_{T,k}}{8} e^{j\theta'_{\text{target},k}} \right. \\
&\qquad \times \{4\pi^2 \delta(\omega_r - \omega_{\text{beat target},k})\delta(\omega_D \pm \omega_{d,k}) \\
&\qquad \left. - e^{-j\pi/2} \Phi_{\text{target},k}(\omega_r - \omega_{\text{beat target},k}, \omega_D \pm \omega_{d,k})\} \right]
\end{aligned} \tag{22}$$

where ω_r and ω_D stand for the angular frequency domains of the range and Doppler, respectively.

IV. Experiments and Radar Systems

In order to demonstrate the aforementioned theories, we conducted two experiments, Experiments A and B, with two radar systems. Both Experiments A and B were carried out on the rooftop of a building. The experimental site shown in Figs. 5 and 6 is where the various causes of the leakage explained in Section I had been verified [10]. The palm-sized small drone, DJI Spark was used as a target. When measuring the ascending and descending Spark with radars, we raised it at a speed of 2.0–2.1 m/s and lowered it at a rate of 1.4–1.5 m/s. The actual velocity of Spark was confirmed through the smart mobile application provided by DJI to help control the drone. The detailed descriptions of each experiment and each radar system follow.

A. Experiment A

In Experiment A, we verified the effect of f_{offset} on the Doppler shift in the r-D map and demonstrate that the proposed method can remove f_{offset} and increase the SNR by reducing the 2-D noise floor. The Ku-band heterodyne FMCW radar used in [10] was used for Experiment A in this article. We intentionally chose this radar system. This system has basically little or no f_{offset}, $f_{\text{random},t}$, and $f_{\text{random},c}$ in the final stage, and it includes a software-defined radio (SDR), Ettus USRP N210, which can provide the fine frequency tuning of an internal LO. Thus, using this device, if we added a virtual f_{offset}, which is assumed to be the one resulting from the carrier frequency errors in all the LOs, to the carrier frequency of the internal LO, there is no other unwanted frequency component except the virtual f_{offset}. This allowed us to clearly verify whether f_{offset} from the carrier frequency error of the LO affected the Doppler shift in the r-D map. The specifications and parameters of the Ku-band heterodyne FMCW radar system are listed in Table I. Fig. 5 shows a scene of Experiment A.

First, we conducted the experiment without the small drone and measured only the leakage signal to evaluate how the proposed method mitigated the 2-D noise floor in the r-D map. Then, we added several virtual f_{offset} by using the SDR to observe the effect of f_{offset} on the Doppler shift. Because this is not the direct injection of the Doppler frequency, if the theoretical analyses in Section II, which argue that the offset frequency causes the problem of the unwanted Doppler shift, are not true, there will be no Doppler shifts. On the other hand, if the theoretical analyses are proven to be true, the Doppler shifts will occur.

Second, with several virtual f_{offset}, we measured both the signals of the leakage and the small moving drone. We raised and lowered the drone and detected it in the r-D map.

By comparing the results for the common method and the proposed method, which were obtained in these experiments,

TABLE I
SPECIFICATIONS AND PARAMETERS OF THE KU-BAND HETERODYNE FMCW RADAR SYSTEM

Parameters	Values (default)
Operating frequency	14.35-14.50 GHz
Transmit power	30 dBm
Antenna gain	16 dBi
Sweep bandwidth (BW)	150 MHz
True range resolution	1 m
Sweep period (T)	880 us
Desired digital bandwidth	1.25 MHz
Minimum available sampling frequency (F_S)	2.5 MHz
Oversampling factor (Q)	4
Oversampling frequency (QF_S)	10 MHz
# of samples in a chirp	8800
# of samples after discarding early part in a chirp	8192
IF carrier frequency ($f_{IF\ carrier}$)	2.5 MHz
Window	Hann
$NFFT$ for finding out $f_{IF\ beat\ leakage}$ and $\theta_{IF\ leakage}$	2^{20}
Desired maximum detectable range	1100 m
Apparent range resolution	1.074 m
# of chirps for one r-D map	256
Velocity resolution	0.0462 m/s

TABLE II
SPECIFICATIONS AND PARAMETERS OF THE X-BAND HETERODYNE FMCW RADAR SYSTEM

Parameters	Values (default)
Operating frequency	11.00-11.15 GHz
Transmit power	0 dBm
Antenna gain	20.75 dBi
Sweep bandwidth (BW)	150 MHz
True range resolution	1 m
Sweep period (T)	1760 us
Desired digital bandwidth	312.5 kHz
Minimum available sampling frequency (F_S)	625 kHz
Oversampling factor (Q)	4
Oversampling frequency (QF_S)	2.5 MHz
# of samples in a chirp	4400
# of samples after discarding early part in a chirp	4096
IF carrier frequency ($f_{IF\ carrier}$)	625 kHz
Window	Hann
$NFFT$ for finding out $f_{IF\ beat\ leakage}$ and $\theta_{IF\ leakage}$	2^{18}
Desired maximum detectable range	550 m
Apparent range resolution	1.074 m
# of chirps for one r-D map	256
Velocity resolution	0.0301 m/s

we can prove whether the proposed method increased the SNR and corrected the velocity error of the small moving drone due to f_{offset} at the same time.

B. Experiment B

In Experiment B, we demonstrated that the proposed method removed the velocity error of the small moving drone due to both f_{offset} and $f_{\text{random},c}$ while simultaneously increasing the SNR in the r-D map. For Experiment B, we used an X-band heterodyne FMCW radar that had a defect. The X-band radar system produced the unwanted random Doppler shift term $f_{\text{offset}} + f_{\text{random},c}$. Note that $f_{\text{random},c}$ is random, and thus, $f_{\text{offset}} + f_{\text{random},c}$ is also random. Though this was basically a bad system, paradoxically, it was quite suitable for Experiment B. If the proposed method proves its capabilities through this experiment, then it means that the X-band radar can be used as a good system, by applying the proposed method.

The specifications and parameters of the X-band heterodyne FMCW radar system are listed in Table II. Fig. 6 shows the X-band heterodyne FMCW radar system and a scene of Experiment B. The detailed block diagram of the X-band heterodyne FMCW radar system is shown in Fig. 7. In the system, a direct digital synthesizer, Analog Device AD9914, is included as the LFM signal generator. For the antennas, typical rectangular horn antennas for X-band were used.

As in Experiment A, we first measured only the leakage signal without the small drone to evaluate how the proposed method reduced the 2-D noise floor in the r-D map. Then, we verified whether the proposed method eliminated $f_{\text{offset}} + f_{\text{random},c}$. Finally, by measuring the small moving drone, we proved whether the proposed method could increase the SNR and provide accurate velocity information of the small moving drone at the same time.

V. RESULTS AND DISCUSSION

A. Results and Discussion for Experiment A

Figs. 8–10 show the results of Experiment A. As shown in Fig. 8(a) and (b), the color throughout the r-D map, which means the level of the 2-D noise floor, is bluer in the r-D map with the proposed method than in the r-D map without the proposed method. In other words, the proposed method is well applied in the r-D map so that it reduces the 2-D noise floor. In order to clearly measure the degree of improvement, we took an average of the r-D maps, which reduced the variance in the 2-D noise floors. For the average process, we used 750 r-D maps for the r-D map without the proposed method and the r-D map with the proposed method. Then, we obtained the difference of the two averaged r-D maps and produced a fit surface. The result is shown in Fig. 8(c). The maximum and the minimum degree of improvement were about 9.9 and 6.7 dB.

In the Ku-band heterodyne FMCW radar system, we adjusted the carrier frequency of the internal LO in the SDR by ± 100 and ± 200 Hz so that the beat signals had a virtual f_{offset} before the ADC. If the suggested theoretical analysis is correct, the Doppler shift should be consistent with the frequency values that we adjusted. The results are shown in Fig. 9. A zoomed-in version of the r-D maps, which focuses on the leakage beat signal, is presented. Zero padding was applied along the Doppler domain to minimize the measurement error caused by insufficient spacing of the FFT. The resulting measurement error of the Doppler frequency due to the spacing of the FFT was about ± 0.07 Hz. The leakage beat signal is of course static. In Fig. 9, however, the r-D maps without the proposed method have some Doppler frequency and look like a moving target. The measured values of the Doppler frequency were the same as those we adjusted with the SDR. Therefore, this verifies that f_{offset} resulting from the carrier frequency errors

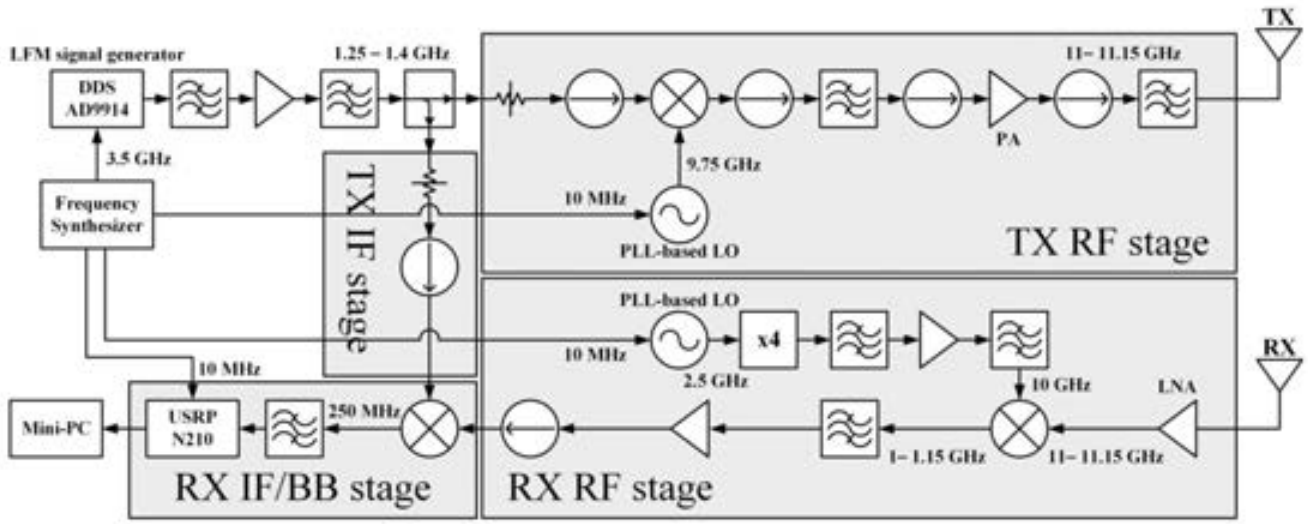

Fig. 7. Block diagram of the X-band heterodyne FMCW radar system.

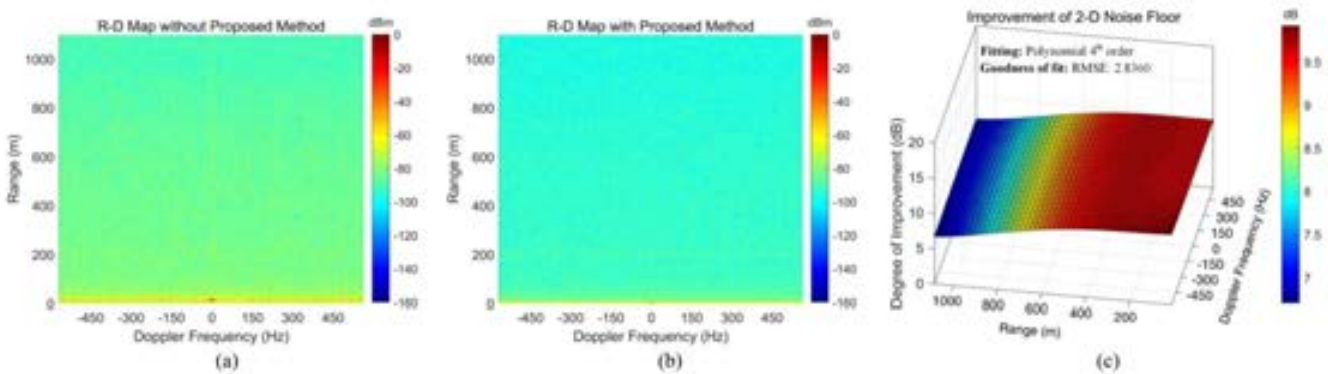

Fig. 8. Results of Experiment A: improvement of the 2-D noise floor. (a) r-D map without the proposed method. (b) r-D map with the proposed method. (c) Degree of improvement.

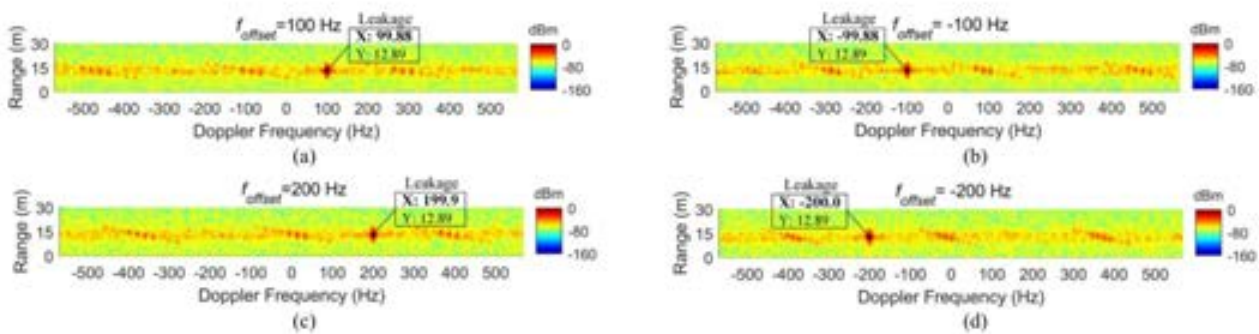

Fig. 9. Results of Experiment A: effect of f_{offset}. Zoomed-in version of r-D maps without the proposed method when (a) $f_{\text{offset}} = 100$ Hz, (b) $f_{\text{offset}} = -100$ Hz, (c) $f_{\text{offset}} = 200$ Hz, and (d) $f_{\text{offset}} = -200$ Hz.

of all the LOs in the heterodyne FMCW radar is directly reflected as the unwanted Doppler shift in the Doppler domain.

The results of the small moving drone measurement are presented in Fig. 10. In the r-D maps without the proposed method [see Fig. 10(a), (c), (e), and (g)], the measured velocity information of the small drone is inaccurate when compared with the actual velocity values in Section IV. They included the velocity error due to f_{offset}, which is $(\lambda/2) \times f_{\text{offset}}$. On the other hand, in Fig. 10(b), (d), (f), and (h), the velocity information of the small drone, which is measured in the r-D maps with the proposed method, corresponds to the accurate velocity information we mentioned in Section IV.

In addition, the measured power values of the small drone in the r-D maps without the proposed method were almost the same as those in the r-D maps with the proposed method.

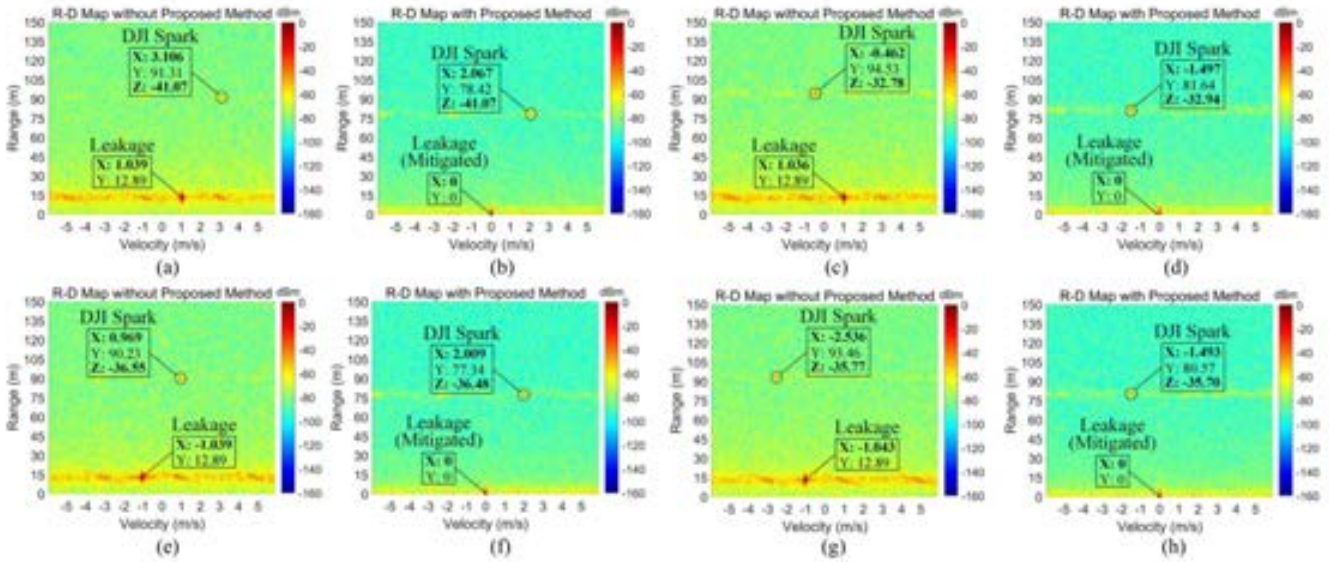

Fig. 10. Results of Experiment A: improvement of r-D map when the small moving drone is detected. (a)–(d) Zoomed-in version of r-D maps when $f_{\text{offset}} = 100$ Hz. (e)–(h) Zoomed-in version of r-D maps when $f_{\text{offset}} = -100$ Hz. (a), (b), (e), and (f) Zoomed r-D maps without/with the proposed method when the small drone is ascending. (c), (d), (g), and (h) Zoomed r-D map without/with the proposed method when the small drone is descending.

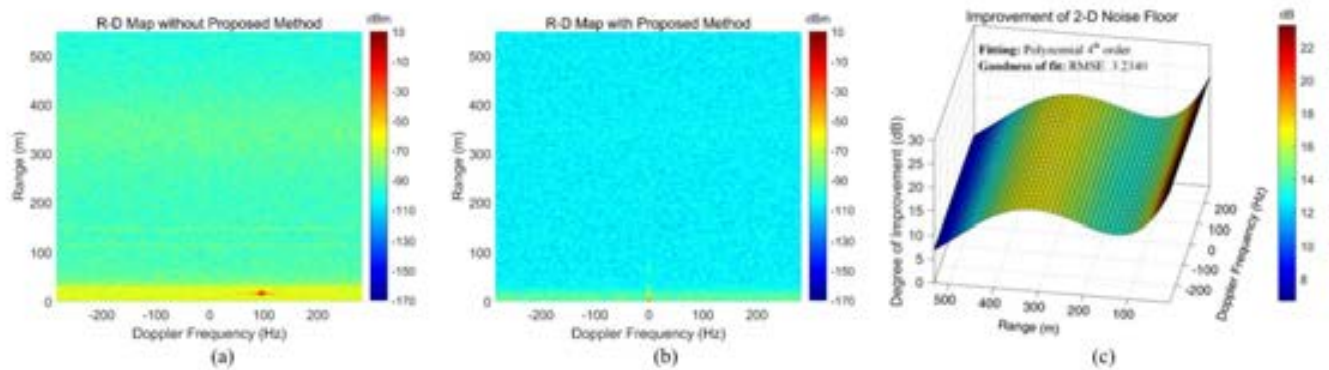

Fig. 11. Results of Experiment B: improvement of the 2-D noise floor. (a) r-D map without the proposed method. (b) r-D map with the proposed method. (c) Degree of improvement.

Namely, the proposed method does not damage the power of the targets. The 2-D noise floor around the target signal is reduced in the r-D map with the proposed method, as we noted in Fig. 8. This proves that the proposed method not only increases the SNR of the small moving drone in the r-D map but also corrects the velocity information by eliminating the unwanted Doppler shift term, f_{offset}.

B. Results and Discussion for Experiment B

The results of Experiment B are shown in Figs. 11–13. The same processes used for Fig. 8 were employed for Fig. 11. In Fig. 11(a) and (b), similar to what we observed in Fig. 8(a) and (b), the color throughout the r-D map with the proposed method is bluer than the one without the proposed method. Namely, according to the color bar, the 2-D noise floor in the r-D map with the proposed method is much lower than the one without the proposed method. The maximum and the minimum degree of improvement were about 23.3 and 6.7 dB.

Fig. 12 shows the experimental results on the unwanted random Doppler shift term, $f_{\text{offset}} + f_{\text{random},c}$. We measured the r-D maps three times and plotted a zoomed-in version of the r-D maps which focuses on the leakage beat signal. As shown in Fig. 12(a), (c), and (e), the leakage beat signals are randomly positioned along the Doppler axis in the r-D maps without the proposed method. On the other hand, in Fig. 12(b), (d), and (f), the leakage beat signals in the r-D maps with the proposed method do not change from measurement to measurement and stay well at the origin.

The results of measuring the small moving drone are shown in Fig. 13. In Fig. 13(a), while in practice, the small drone is moving away from the radar with the speed of 2.0–2.1 m/s, the r-D map without the proposed method indicates that the small drone is approaching the radar, and its speed is about 3.3 m/s. In contrast, the r-D map using the proposed method in Fig. 13(b) indicates the accurate state of the small moving drone. For Fig. 13(c) and (d), in practice, the small drone is approaching the radar with a speed of 1.4–1.5 m/s.

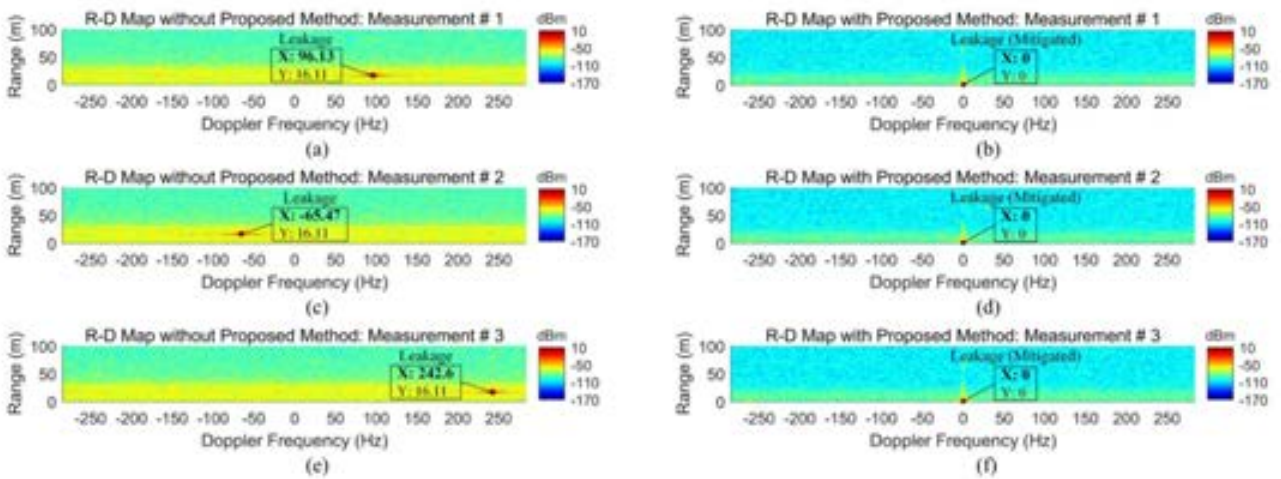

Fig. 12. Results of Experiment B: effect and removal of the unwanted random Doppler shift. Zoomed-in version of r-D maps without the proposed method at (a) measurement # 1, (c) measurement # 2, and (e) measurement # 3. r-D maps with the proposed method at (b) measurement # 1, (d) measurement # 2, and (f) measurement # 3.

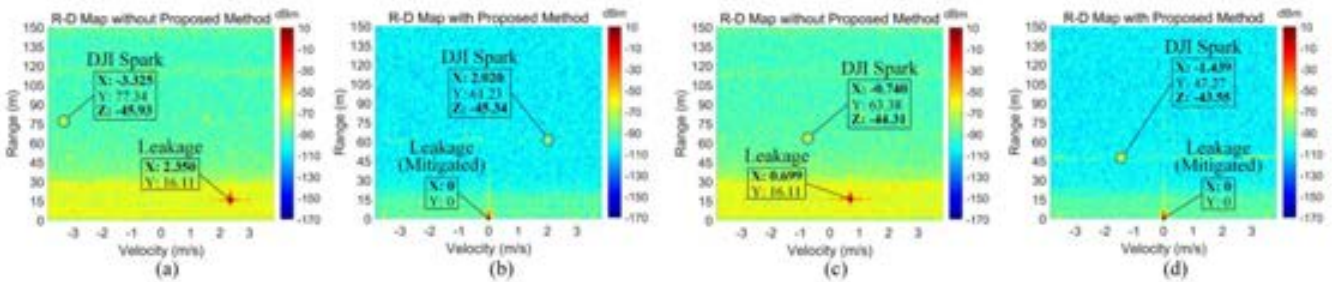

Fig. 13. Results of Experiment B: improvement of r-D map when the small moving drone is detected. (a)–(d) Zoomed-in version of r-D maps. (a) and (b) Zoomed r-D maps without/with the proposed method when the small drone is ascending. (c) and (d) Zoomed r-D map without/with the proposed method when the small drone is descending.

However, the r-D map without the proposed method in Fig 13(c) indicates that the small drone is approaching the radar with a speed of 0.7 m/s. On the other hand, the r-D map with the proposed method in Fig. 13(d) indicates the accurate state of the small moving drone. Also, as we have observed in the results of Experiment A, the measured power values of the small drone are almost the same in both r-D maps with and without the proposed method. The 2-D noise floor around the small drone signal, however, is much lower in the r-D map with the proposed method than in the r-D map without the proposed method.

Therefore, this confirms that the proposed method increases the SNR of the small moving drone in the r-D map and provides accurate velocity information by removing the unwanted random Doppler shift term, $f_{\text{offset}} + f_{\text{random},c}$. Furthermore, although the problematic X-band radar system was useless in detecting the small moving drone through the r-D map, it has been changed to an excellent and reliable radar system even without additional hardware parts due to the proposed method. Finally, the proposed method can be compared with the existing methods in Table III. As shown in Table III, we have performed the significant improvement of the 2-D noise floor in the r-D map and the velocity error correction simultaneously without additional hardware parts for the first time in this article.

C. Prospective Applications of Proposed Method

The r-D map is widely employed in the FMCW radar not only for moving target detection but also for many other radar applications. For example, motion detection and recognition can be performed based on the r-D map [36], [43]. In meteorological radars, the r-D map is a source for data processing, including reflectivity profiles of precipitation, rain rate, and so on [44], [45]. In addition, the 2-D FFT is one of the processes in the range-Doppler algorithm (RDA) of synthetic aperture radar (SAR) [46]. Inverse SAR (ISAR) basically produces an r-D map as a result of imaging [47]. Now that the proposed method has been proven to improve the r-D map, we expect that the proposed method can contribute to better results in these various other r-D map applications.

In addition, because all the unwanted frequency and phase terms caused in the radar system are eliminated using the proposed method, the beat signals have coherency. Therefore, the proposed method can contribute to coherent applications, such as coherent integration, moving target indication, static clutter suppression, and so on.

TABLE III
COMPARISON OF THE EXISTING METHODS AND THE PROPOSED METHOD

Paper	Solution	Maximum Improvement Record in Leakage Cancelation/Mitigation	Requirement of Additional Hardware Parts	Additional Features
[22]	Closed-loop leakage canceller	40 dB (Sweep signal in power spectrum at RF stage)	Required	None
[23]	Closed-loop leakage canceller	40 dB (Sweep signal in power spectrum at RF stage)	Required	None
[24]	Closed-loop leakage canceller	45 dB (1-D noise floor in power spectrum at RF stage)	Required	None
[25]	Closed-loop leakage canceller	30 dB (Sweep signal in power spectrum at RF stage)	Required	None
[27]	Leakage canceller topology based on microstrip line application	40.5 dB (avg.) (TX-to-RX isolation at RF stage)	Required	None
[28]	Leakage canceller topology based on microstrip line application	28.2 dB (TX-to-RX isolation at RF stage)	Required	None
[29]	Leakage canceller topology based on microstrip line application	35.27 dB (TX-to-RX isolation at RF stage)	Required	None
[30]	Artificial on-chip target	6.4 dB (simulation) (1-D noise floor in power spectrum at baseband) (final signal processing result)	Required	None
[31]	Artificial on-chip target	5 dB (1-D noise floor in power spectrum at baseband) (final signal processing result)	Required	None
[10]	SPC technique	10.5 dB (1-D noise floor in power spectrum at baseband) (final signal processing result)	Not required	Range error correction (internal delay compensation)
Proposed method	SPC technique	23.3 dB (2-D noise floor in r-D map at baseband) (final signal processing result)	Not required	Range error correction (internal delay compensation), velocity error correction (phase calibration)

VI. CONCLUSION

Detailed theoretical analyses of the practical problems encountered with heterodyne FMCW radar, which degrade the performance of the r-D map, have been provided. In the r-D map, the phase noise of leakage increases the 2-D noise floor, and the unwanted Doppler shift terms change the measured velocity information of a small moving drone. In order to resolve these practical problems and improve the r-D map, the upgraded theory and realization method of the SPC technique have been proposed. The experimental results demonstrated that the proposed method decreased the 2-D noise floor in the r-D map by mitigating the phase noise of the leakage. In addition, it was verified that the proposed method removes the unwanted Doppler shift terms by calibrating the unwanted phases in the beat signals of each chirp. Finally, it was proven that the proposed method improves the SNR of

the small moving drone in the r-D map and provides accurate velocity information at the same time. Because the r-D map is also used in many radar applications other than moving target detection, the proposed method can also contribute to those applications. In addition, the proposed method can also be used for coherent radar applications, since it makes the FMCW radar coherent.

REFERENCES

[1] W. Ripley. (Apr. 22, 2015). *Drone With Radioactive Material Found on Japanese Prime Minister's Roof*. CNN. Accessed: Jul. 14, 2019. [Online]. Available: https://edition.cnn.com/2015/04/22/asia/japan-prime-minister-rooftop-drone/index.html

[2] P. Phillips. (Feb. 15, 2018). *Charleston Helicopter Crash Blamed on Drone; FAA Investigating*. Live 5 News. Accessed: Jul. 14, 2019. [Online]. Available: https://www.live5news.com/story/37518601/charleston-helicopter-crash-blamed-on-drone-faa-investigating/

[3] J. Rowlatt. (Apr. 14, 2015). *Gatwick Drone Attack Possible Inside Job, Say Police*. BBC News. Accessed: Jul. 14, 2019. [Online]. Available: https://www.bbc.com/news/uk-47919680

[4] J. Drozdowicz *et al.*, "35 GHz FMCW drone detection system," in *Proc. 17th Int. Radar Symp.*, May 2016, pp. 1–4.

[5] J. Lee, M. Park, I. Eo, and B. Koo, "An X-band FMCW radar for detection and tracking of miniaturized UAVs," in *Proc. Int. Conf. Comput. Sci. Comput. Intell.*, Las Vegas, NV, USA, Dec. 2017, pp. 1844–1845.

[6] T. Multerer *et al.*, "Low-cost jamming system against small drones using a 3D MIMO radar based tracking," in *Proc. 14th Eur. Radar Conf.*, Nuremberg, Germany, Oct. 2017, pp. 299–302.

[7] J. Park and S.-O. Park, "A down-conversion method for attenuation of leakage signal in FMCW radar," in *Proc. Int. Symp. Antennas Propag.*, Phuket, Thailand, Oct. 2017, pp. 1–2.

[8] Y. Dobrev *et al.*, "Radar-based high-accuracy 3D localization of UAVs for landing in GNSS-denied environments," in *IEEE MTT-S Int. Microw. Symp. Dig.*, Apr. 2018, pp. 1–4.

[9] Y. Wang, T. Phelps, K. Kibaroglu, M. Sayginer, Q. Ma, and G. M. Rebeiz, "28 GHz 5G-based phased-arrays for UAV detection and automotive traffic-monitoring radars," in *IEEE MTT-S Int. Microw. Symp. Dig.*, Philadelphia, PA, USA, Jun. 2018, pp. 895–898.

[10] J. Park, S. Park, D.-H. Kim, and S.-O. Park, "Leakage mitigation in heterodyne FMCW radar for small drone detection with stationary point concentration technique," *IEEE Trans. Microw. Theory Techn.*, vol. 67, no. 3, pp. 1221–1232, Mar. 2019.

[11] B. Razavi, "Design considerations for direct-conversion receivers," *IEEE Trans. Circuits Syst. II, Analog Digit. Signal Process.*, vol. 44, no. 6, pp. 428–435, Jun. 1997.

[12] M. Nalezinski, M. Vossiek, and P. Heide, "Novel 24 GHz FMCW front-end with 2.45 GHz SAW reference path for high-precision distance measurements," in *IEEE MTT-S Int. Microw. Symp. Dig.*, Jun. 1997, pp. 185–188.

[13] C. Pfeffer, R. Feger, C. M. Schmid, C. Wagner, and A. Stelzer, "An IQ-modulator based heterodyne 77-GHz FMCW colocated MIMO radar system," in *IEEE MTT-S Int. Microw. Symp. Dig.*, Jun. 2012, pp. 1–3.

[14] K.-B. Kong, W.-R. Jeong, and S.-O. Park, "Design and initial measurements of K-band FMCW rain radar with high resolution," *Microw. Opt. Technol. Lett.*, vol. 58, no. 4, pp. 817–822, Apr. 2016.

[15] T. Saito, N. Okubo, Y. Kawasaki, O. Isaji, and H. Suzuki, "An FM-CW radar module with front-end switching heterodyne receiver," in *IEEE MTT-S Int. Microw. Symp. Dig.*, vol. 2, Jun. 1992, pp. 713–716.

[16] D. C. W. Lo *et al.*, "A single-chip W-band transceiver with front-end switching receiver for FMCW radar applications," in *IEEE MTT-S Int. Microw. Symp. Dig.*, vol. 2, May 1995, pp. 873–876.

[17] R. J. Dengler *et al.*, "600 GHz imaging radar with 2 cm range resolution," in *IEEE MTT-S Int. Microw. Symp. Dig.*, Honolulu, HI, USA, Jun. 2007, pp. 1371–1374.

[18] K. B. Cooper *et al.*, "A high-resolution imaging radar at 580 GHz," *IEEE Microw. Wireless Compon. Lett.*, vol. 18, no. 1, pp. 64–66, Jan. 2008.

[19] K. B. Cooper, R. J. Dengler, N. Llombart, B. Thomas, G. Chattopadhyay, and P. H. Siegel, "THz imaging radar for standoff personnel screening," *IEEE Trans. Terahertz Sci. Technol.*, vol. 1, no. 1, pp. 169–182, Sep. 2011.

[20] B. Boukari, E. Moldovan, S. Affes, K. Wu, R. G. Bosisio, and S. O. Tatu, "A heterodyne six-port FMCW radar sensor architecture based on beat signal phase slope techniques," *Prog. Electromagn. Res.*, vol. 93, pp. 307–322, Jul. 2009.

[21] M.-T. Dao, D.-H. Shin, Y.-T. Im, and S.-O. Park, "A two sweeping VCO source for heterodyne FMCW radar," *IEEE Trans. Instrum. Meas.*, vol. 62, no. 1, pp. 230–239, Jan. 2013.

[22] P. D. L. Beasley, A. G. Stove, B. J. Reits, and B. As, "Solving the problems of a single antenna frequency modulated CW radar," in *Proc. IEEE Int. Conf. Radar*, Arlington, VA, USA, May 1990, pp. 391–395.

[23] K. Lin, R. H. Messerian, and Y. Wang, "A digital leakage cancellation scheme for monostatic FMCW radar," in *IEEE MTT-S Int. Microw. Symp. Dig.*, vol. 2, Jun. 2004, pp. 747–750.

[24] K. Lin and Y. E. Wang, "Transmitter noise cancellation in monostatic FMCW radar," in *IEEE MTT-S Int. Microw. Symp. Dig.*, Jun. 2006, pp. 1406–1409.

[25] K. Lin, Y. E. Wang, C.-K. Pao, and Y.-C. Shih, "A Ka-band FMCW radar front-end with adaptive leakage cancellation," *IEEE Trans. Microw. Theory Techn.*, vol. 54, no. 12, pp. 4041–4048, Dec. 2006.

[26] M. Yuehong, L. Qiusheng, and Z. Xiaolin, "Research on carrier leakage cancellation technology of FMCW system," in *Proc. 18th Int. Conf. Adv. Commun. Technol.*, Pyeongchang, South Korea, 2016, pp. 7–9.

[27] J.-G. Kim, S. Ko, S. Jeon, J.-W. Park, and S. Hong, "Balanced topology to cancel Tx leakage in CW radar," *IEEE Microw. Wireless Compon. Lett.*, vol. 14, no. 9, pp. 443–445, Sep. 2004.

[28] C. Kim *et al.*, "Tx leakage cancellers for 24 GHz and 77 GHz vehicular radar applications," in *IEEE MTT-S Int. Microw. Symp. Dig.*, Jun. 2006, pp. 1402–1405.

[29] C.-Y. Kim, J.-G. Kim, and S. Hong, "A quadrature radar topology with Tx leakage canceller for 24-GHz radar applications," *IEEE Trans. Microw. Theory Techn.*, vol. 55, no. 7, pp. 1438–1444, Jul. 2007.

[30] A. Melzer, A. Onic, F. Starzer, and M. Huemer, "Short-range leakage cancelation in FMCW radar transceivers using an artificial on-chip target," *IEEE J. Sel. Top. Signal Process.*, vol. 9, no. 8, pp. 1650–1660, Dec. 2015.

[31] A. Melzer, F. Starzer, H. Jäger, and M. Huemer, "Real-time mitigation of short-range leakage in automotive FMCW radar transceivers," *IEEE Trans. Circuits Syst. II, Exp. Briefs*, vol. 64, no. 7, pp. 847–851, Jul. 2017.

[32] A. Wojtkiewicz, J. Misiurewicz, M. Nalecz, K. Jedrzejewski, and K. Kulpa, "Two-dimensional signal processing in FMCW radars," in *Proc. 20th Nat. Conf. Circuit Theory Electron. Netw.*, vol. 2, 1997, pp. 475–480.

[33] F. Ali and M. Vossiek, "Detection of weak moving targets based on 2-D range-Doppler FMCW radar Fourier processing," in *German Microw. Conf. Dig. Papers*, Berlin, Germany, 2010, pp. 214–217.

[34] K. Thurn, D. Shmakov, G. Li, S. Max, M.-M. Meinecke, and M. Vossiek, "A novel interlaced chirp sequence radar concept with range-Doppler processing for automotive applications," in *IEEE MTT-S Int. Microw. Symp. Dig.*, May 2015, pp. 1–4.

[35] K. Thurn, D. Shmakov, G. Li, S. Max, M. M. Meinecke, and M. Vossiek, "Concept and implementation of a PLL-controlled interlaced chirp sequence radar for optimized range-Doppler measurements," *IEEE Trans. Microw. Theory Techn.*, vol. 64, no. 10, pp. 3280–3289, Oct. 2016.

[36] Z. Peng, C. Li, J.-M. Muñoz-Ferreras, and R. Gómez-García, "An FMCW radar sensor for human gesture recognition in the presence of multiple targets," in *IEEE MTT-S Int. Microw. Symp. Dig.*, May 2017, pp. 1–3.

[37] Norsat. *1000 Ku-Band Single Band PLL LNB*. HS1000. datasheet. Accessed: Nov. 12, 2019. [Online]. Available: https://products.norsat.com/UserFiles/NorsatDocs/HS1000%20Spec%20Sheet.pdf

[38] XMW. *Ku-Band PLL LNB*. R1000IA. datasheet. Accessed: Nov. 12, 2019. [Online]. Available: http://www.xmwinc.com/_download.php?filekeyname=1484032220qv85i0tzb6p2cx0.pdf&filename=R1000IA-Ku-band%20PLL%20LNB

[39] XMW. *Ka-Band PLL LNB*. R9000IA. datasheet. Accessed: Nov. 12, 2019. [Online]. Available: http://www.xmw.co.kr/_download.php?filekeyname=1484031792yth82842h53i2m75.pdf&filename=R9000IA-Ka-band%20PLL%20LNB

[40] B. Razavi, "Challenges in the design of frequency synthesizers for wireless applications," in *Proc. IEEE Custom Integr. Circuits Conf.*, May 1997, pp. 395–402.

[41] K. Czuba and D. Sikora, "Temperature stability of coaxial cables," *Acta Phys. Pol. A*, vol. 119, no. 4, pp. 553–557, Apr. 2011.

[42] M. Le Breton *et al.*, "Outdoor UHF RFID: Phase stabilization for real-world applications," *IEEE J. Radio Freq. Identificat.*, vol. 1, no. 4, pp. 279–290, Dec. 2017.

[43] S. Fukushima, H. Yamada, H. Kobayashi, and Y. Yamaguchi, "Human motion detection and extraction by using FM-CW range-Doppler radar," in *Proc. Int. Symp. Antennas Propag. Conf.*, Kaohsiung, Taiwan, Dec. 2014, pp. 173–174.

[44] A. Leuenberger, "Precipitation measurements with microwave sensors," M.S. thesis, Dept. Sci., Univ. Bern, Bern, Switzerland, 2009.
[45] M. He, Y. Nian, X. Wang, S. Xiao, and Y. Li, "Improved clutter suppression algorithm for atmospheric target detection using polarimetric Doppler radar," *IEEE J. Sel. Top. Appl. Earth Observ. Remote Sens.*, vol. 4, no. 4, pp. 911–922, Dec. 2011.
[46] J. Dewit, A. Meta, and P. Hoogeboom, "Modified range-Doppler processing for FM-CW synthetic aperture radar," *IEEE Geosci. Remote Sens. Lett.*, vol. 3, no. 1, pp. 83–87, Jan. 2006.
[47] E. Giusti and M. Martorella, "Range Doppler and image autofocusing for FMCW inverse synthetic aperture radar," *IEEE Trans. Aerosp. Electron. Syst.*, vol. 47, no. 4, pp. 2807–2823, Oct. 2011.

Junhyeong Park (Graduate Student Member, IEEE) received the B.S. and M.S. degrees in electrical engineering from the Korea Advanced Institute of Science and Technology (KAIST), Daejeon, South Korea, in 2015 and 2017, respectively, where he is currently pursuing the Ph.D. degree in electrical engineering.

His current research interests include radar systems for defense, drone detection radar, radar imaging, target recognition/classification, and radar signal processing.

Dae-Hwan Jung was born in Seoul, South Korea, in 1988. He received the B.S. degree in electronic and electrical engineering from Sungkyunkwan University, Suwon, South Korea, in 2014, and the M.S. degree in electrical engineering from the Korea Advanced Institute of Science and Technology, Daejeon, South Korea, in 2016, where he is currently pursuing the Ph.D. degree.

His current research interests include the design of frequency-modulated continuous-wave (FMCW) radar systems, FMCW synthetic aperture radar (SAR), and SAR signal processing.

Kyung-Bin Bae received the B.S. degree from the Department of Electronic Engineering, Pusan National University, Busan, South Korea, in 2011, and the M.S. degree in electrical engineering from the Pohang University of Science and Technology, Pohang, South Korea, in 2013. He is currently pursuing the Ph.D. degree at the School of Electrical Engineering, Korea Advanced Institute of Science and Technology, Daejeon, South Korea.

His current research interests include beamforming network, multi-in multi-out (MIMO) channel capacity, and frequency-modulated continuous-wave radar systems.

Seong-Ook Park (Senior Member, IEEE) was born in Yeongcheon, South Korea, in 1964. He received the B.S. degree in electrical engineering from Kyungpook National University, Daegu, South Korea, in 1987, the M.S. degree in electrical engineering from the Korea Advanced Institute of Science and Technology, Daejeon, South Korea, in 1989, and the Ph.D. degree in electrical engineering from Arizona State University, Tempe, AZ, USA, in 1997.

From 1989 to 1993, he was a Research Engineer with Korea Telecom, Daejeon, where he was involved in microwave systems and networks. He then was with the Telecommunication Research Center, Arizona State University, until 1997. Since 1997, he has been a Professor with the Korea Advanced Institute of Science and Technology. His current research interests include antenna, radar system, and analytical and numerical techniques in the area of electromagnetics.

Dr. Park is a member of the Pi Kappa Phi.